

Biaxial Strain Modulation of Exciton-Phonon Resonance in WS₂

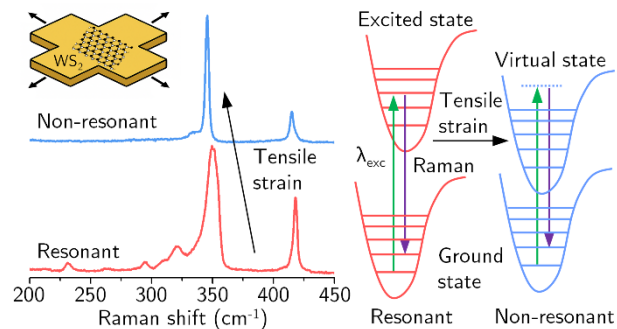
Álvaro Rodríguez^{1†*}, Carmen Munuera¹, Andres Castellanos-Gomez¹

¹Instituto de Ciencia de Materiales de Madrid (ICMM-CSIC), C. Sor Juana Inés de la Cruz, 3, Madrid, 28049, Spain.

*Corresponding author(s): alvaro.rodriguez@csic.es

Keywords: strain engineering, transition metal dichalcogenides, resonant Raman spectroscopy, exciton-phonon coupling, gold-assisted exfoliation

TOC Graphic



ABSTRACT

Mechanical strain provides a powerful route to tune light-matter interactions in two-dimensional semiconductors, yet the impact of biaxial strain on resonant Raman scattering remains poorly quantified. Here we use a cruciform bending platform to apply uniform biaxial strain up to 1.3% to trilayer WS₂ while simultaneously monitoring excitonic and vibrational responses. Differential

reflectance reveals strain-induced red-shifts of the A and B excitons, with the B exciton moving by about 170 meV. Under 532 nm excitation, this shift drives a continuous transition from resonant to non-resonant Raman scattering, leading to a pronounced collapse of the 2LA(M) mode. The 2LA(M) intensity is quantitatively described by a resonance model expressed in terms of the B-exciton energy, which yields an effective exciton-assisted linewidth of about 34 meV and shows that the maximum enhancement occurs when the laser lies roughly 50 meV below the exciton. The first-order phonons remain narrow and reversible over the full strain cycle, confirming elastic deformation and efficient isotropic strain transfer. Our results establish biaxial strain as a practical and reversible route to modulate exciton-phonon coupling and Raman scattering cross-sections, enabling mechanically reconfigurable optical and photonic functionalities in layered semiconductors.

Introduction

Transition metal dichalcogenides (TMDs) combine tightly bound excitons with strong electron-phonon interactions, which makes them promising materials for optoelectronic and photonic technologies where optical responses can be dynamically tuned.¹⁻³ Mechanical strain modifies their electronic structure and excitonic resonances, with uniaxial deformation widely used to shift bandgaps, alter exciton diffusion, and control valley polarization.⁴⁻⁹ In contrast, applying homogeneous biaxial strain remains challenging because achieving uniform in-plane expansion without shear is experimentally demanding, particularly over large areas.¹⁰⁻¹³

Several approaches have been developed to impose biaxial strain on TMDs, including bubble pressurization, suspended membrane deformation, thermal expansion mismatch, and substrate

engineering.^{14–18} Although effective under specific conditions, these strategies often introduce strain gradients, complex deformation fields, or local dielectric variations that complicate the interpretation of excitonic and vibrational responses. Attempts based on bending geometries have typically been limited to small strain values or have suffered from inefficient strain transfer, further restricting quantitative analysis. As a result, most previous work has focused on photoluminescence shifts or bandgap renormalization, whereas the impact of homogeneous biaxial strain on resonant Raman scattering and exciton-phonon coupling has remained unexplored.^{19–22}

Recently, we demonstrated that directly exfoliating MoS₂ onto ultrathin gold films markedly improves strain-transfer efficiency and increases the maximum achievable strain in uniaxial experiments. Building on this concept, TMDs on gold may overcome these limitations and enable the controlled application of homogeneous biaxial strain.

Raman scattering in TMDs is strongly enhanced when the excitation energy matches an excitonic transition. Under resonance, both first-order phonons and intervalley double-resonant modes such as 2LA(M) become particularly intense.^{23–26} Since strain shifts exciton energies, it should enable direct and reversible modulation of Raman cross-sections. However, a quantitative demonstration that links strain-driven exciton shifts to the suppression of double-resonant scattering has been missing.

In this work, we apply homogeneous biaxial strain to trilayer WS₂ using a cruciform bending platform that provides efficient and isotropic strain transfer across regions of several hundred microns.¹⁰ WS₂ flakes obtained by gold-assisted exfoliation retain their optical quality and adhere strongly to the polymer substrate, enabling simultaneous tracking of exciton energies and

Raman modes up to very high strain values.^{27–30} We show that biaxial tensile strain continuously red-shifts the A and B excitons and drives a transition from resonant to non-resonant Raman scattering as the B exciton energy moves away from the laser excitation energy. The collapse of the 2LA(M) band is quantitatively described by a resonance model formulated in terms of the exciton energy and the finite width of the exciton-assisted double-resonant window. Our results establish biaxial strain as a practical and reversible route to engineer Raman resonance and exciton-phonon coupling in layered semiconductors.

To our knowledge, this is the first quantitative demonstration that homogeneous biaxial strain can drive a controlled transition between resonant and non-resonant Raman scattering in a layered semiconductor. The same strategy can be applied to a broad class of van der Waals heterostructures where exciton-mediated Raman processes are relevant.

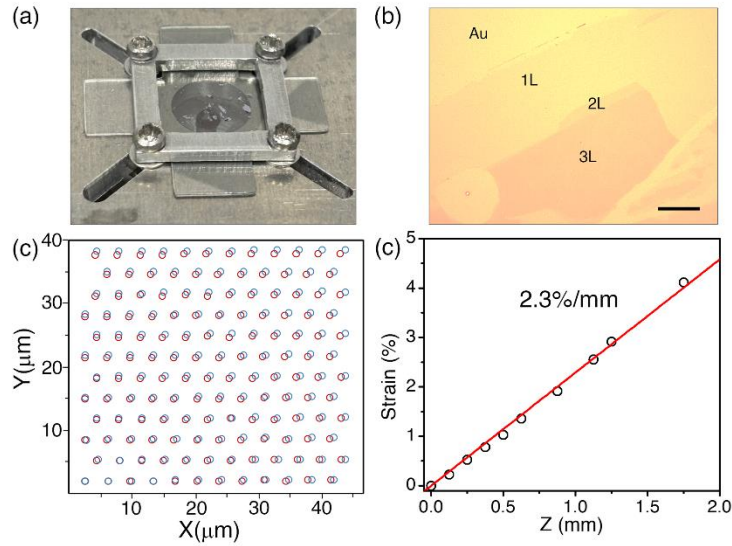


Figure 1. Experimental configuration and strain calibration. (a) Photograph of the cross-shaped flexible polycarbonate (PC) substrate used to apply biaxial strain. The central region hosts the large WS₂ layers. (b) Optical micrograph of the WS₂ monolayer, bilayer and trilayer regions on Au/PC. Scale bar is 10 μm. (c) Pillar-array calibration of the biaxial strain. Optical images collected before and after bending at 2% strain reveal isotropic expansion of pillar spacing. (d) Strain extracted from pillar displacements as a function of Z-stage position (Z). The linear fit ($\epsilon = kZ$) provides the calibration used throughout this work.

To impose homogeneous biaxial strain, we use a cruciform bending geometry in which WS₂ is positioned on the tensile side of a cross-shaped polycarbonate (PC) substrate^{10,31,32} (Figure 1(a) and Figure S1). Out-of-plane bending produces isotropic in-plane expansion in the central region, enabling uniform biaxial deformation over large areas while minimizing shear. Large WS₂ flakes were obtained by Au-assisted exfoliation, which provides clean interfaces and strong adhesion to the substrate, as shown in Figure 1(b). Trilayer WS₂ was chosen because its excitonic resonances remain well resolved in differential reflectance under strain, even when supported on Au. Additional datasets for monolayer and bilayer WS₂ are provided in the Supporting Information (Figure S2).

Strain calibration was performed using a pillar-array reference patterned on an identical substrate. The in-plane strain was extracted from the fractional change in pillar spacing before and after bending at 2% strain (Figure 1(c)). As expected for the bending geometry, the strain increases linearly with the Z-stage displacement (Figure 1(d)) and this calibration was used to convert all displacements into absolute biaxial strain values. The isotropy of the strain field is supported by the linear softening of both in-plane (E) and out-of-plane (A₁) phonon modes (Figure 3). We adopt the E and A₁ notation for the in-plane and out-of-plane Raman modes, respectively, consistent with the symmetry reduction of the WS₂-Au heterostructure to the C_{3v} point group.³³

Figure 2 shows the Raman response of trilayer WS₂ under 532 nm excitation, which lies near the B-exciton energy and enhances both first-order and double-resonant processes. The E phonon appears at $\approx 355 \text{ cm}^{-1}$ and A₁ phonon at $\approx 417 \text{ cm}^{-1}$ accompanied by a strong 2LA(M) band.^{34,35} Their partial overlap produces an asymmetric profile that serves as a sensitive reference for tracking the evolution of exciton-phonon coupling under biaxial strain.^{24,26}

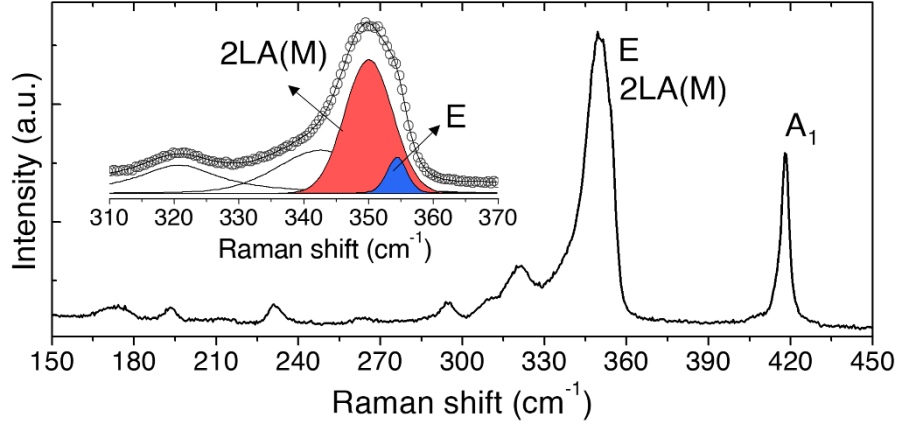


Figure 2. Resonant Raman features in trilayer WS₂ under 532 nm excitation. Raman spectrum at zero strain ($\epsilon = 0\%$) showing the resonant enhancement of the 2LA(M) band. The spectral decomposition highlights contributions from the E, A₁, and 2LA(M) modes obtained by multi-peak fitting (pseudo-Voigt profiles). Peaks labels and color-match those used in the strain-dependent measurements. Overlap between the E phonon and the double-resonant 2LA(M) mode produces an asymmetric band whose intensity and shape are highly sensitive to exciton-mediated resonance.

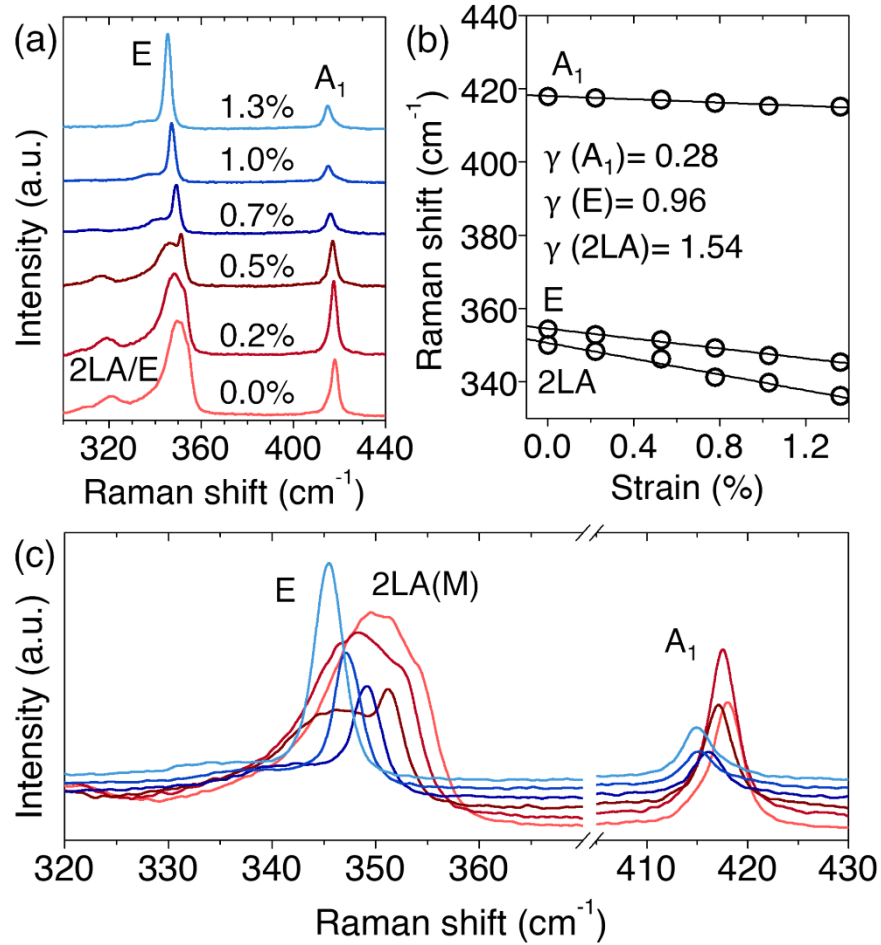


Figure 3. Phonon softening and resonant Raman evolution in biaxially strained WS₂. (a) Raman spectra of trilayer WS₂ acquired at increasing biaxial strain. (b) Strain dependence of the E, A₁, and 2LA(M) phonon frequencies. Linear fits yield slopes of -6.8 ± 0.10 cm⁻¹/%, and -2.3 ± 0.08 cm⁻¹/%, and -10.8 ± 0.6 cm⁻¹/% respectively. Using $\gamma = -\frac{1}{2\omega_0} \left(\frac{d\omega}{d\varepsilon} \right)$, we obtain the Grüneisen parameter for each Raman mode. $\gamma(E) = 0.96 \pm 0.05$, $\gamma(A_1) = 0.28 \pm 0.03$ and $\gamma(2LA) = 1.5 \pm 0.15$. (c) Zoomed view of the spectra highlighting red-shifts and the reduction of resonant enhancement.

Figure 3(a) shows Raman spectra recorded between 0 and 1.3% biaxial strain. Both first-order phonons red-shift systematically, with the E mode exhibiting the stronger dependence. This behavior is characteristic of biaxial deformation: the E mode, involving in-plane motion, responds more strongly to isotropic expansion, whereas the out-of-plane A₁ mode shows a more modest softening.¹² Under uniaxial deformation, the A₁ mode undergoes a markedly smaller

shift, while the E mode splits into two components.^{4,9} A closer view of the E, A₁ and 2LA(M) region (Figure 3(c)) highlights the simultaneous red-shift of the phonons and the progressive reduction of the 2LA(M) enhancement as strain increases. The phonon frequencies extracted from multi-peak fits are plotted in Figure 3(b). From linear fits, we obtain gauge factors of $\frac{d\omega_E}{d\varepsilon} = -6.8 \pm 0.10 \text{ cm}^{-1}/\%$ and $\frac{d\omega_{A_1}}{d\varepsilon} = -2.3 \pm 0.08 \text{ cm}^{-1}/\%$. Comparable values were found for monolayer and bilayer WS₂ (Figure S2). The strain sensitivity of each phonon can be expressed in terms of its Grüneisen parameter (γ), a dimensionless measure of how vibrational frequencies respond to changes in lattice spacing.^{36,37} For biaxial strain, $\gamma = -\frac{1}{2\omega_0} \frac{d\omega}{d\varepsilon}$, where ω_0 is the unstrained phonon frequency. Using the experimental slopes and the unstrained Raman frequencies of the E ($\approx 355 \text{ cm}^{-1}$) and A₁ ($\approx 417 \text{ cm}^{-1}$) modes, we obtain $\gamma(E) = 0.96 \pm 0.05$ and $\gamma(A_1) = 0.28 \pm 0.03$, consistent with efficient isotropic strain transfer and the expected stronger in-plane bond-stretching response of the E mode. These values closely match previous reports for monolayer WS₂ under biaxial strain, where $\gamma(E) \approx 0.85-1.4$ and $\gamma(A_1) \approx 0.22-0.4$ were reported^{12,21}. Importantly, the higher strain values attainable in our samples (up to 1.3% compared to 0.5-0.7% in earlier works) allow us to clearly resolve the intensity decrease of the 2LA(M) mode.

Differential-reflectance spectra in Figure 4(a) reveal a clear red-shift of both A and B excitons with increasing biaxial strain. At high strain, the A-exciton develops a shoulder attributed to an enhanced trion contribution, whereas the B exciton shows no apparent splitting across the full strain range.^{16,22} Each spectrum was subjected to background subtraction to facilitate comparison. The raw spectra can be found in Figure S3 of the Supporting Information. Linear

fits in Figure 4(b) yield shift rates of -150 meV/% for the A exciton and -139 meV/% for the B exciton, the latter reaching a total displacement of ≈ 170 meV at 1.3% strain. These values are consistent with established biaxial strain coefficients in monolayer WS_2 , where the A exciton typically red-shifts by ≈ -130 meV/%.^{11,12,16,38,39} Notably, our strain window is sufficiently large to capture excitonic shifts exceeding the highest reported values in earlier studies.

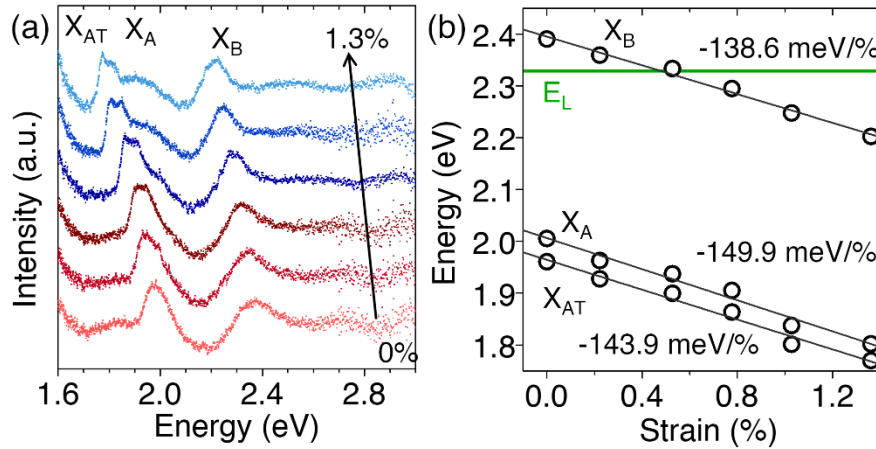


Figure 4. Differential-reflectance tracking of exciton energies under biaxial strain. (a) Normalized $\Delta R/R$ spectra showing the systematic red-shift of the A and B excitons with increasing tensile biaxial strain. The background signal was subtracted from each spectrum for clarity. The raw spectra without background subtraction are displayed in Figure S3 of the Supporting Information. (b) Strain dependence of the X_A , X_B , and X_{AT} energies. Linear fits yield a slope of -138.6 ± 10 meV/% for the B exciton, corresponding to a total shift of ≈ 170 meV at $\epsilon = 1.3\%$. The green line marks the laser excitation energy (E_L).

Because the Raman excitation (532 nm, 2.33 eV) initially lies within the excitonic resonance region, the strain-induced red-shifts of the A and B excitons lead to a progressive increase in the energy mismatch between the B exciton and the laser (Figure 5(a)). This spectral separation coincides directly with the suppression of the 2LA(M) band, establishing a clear link between the electronic and vibrational responses under controlled biaxial expansion (Figure 5(b)).

The 2LA(M) mode arises from a double-resonant intervalley scattering pathway involving virtual states near the excitonic transition. Because the efficiency of this process depends sensitively on the proximity between the laser energy and the exciton, any displacement of the exciton energy modifies the Raman cross-section. When the laser excitation matches an excitonic absorption, the density of accessible intermediate states and the probability of populating them increase markedly, enhancing the double-resonant scattering and making the 2LA(M) mode much more intense. Under tensile biaxial strain, the red-shift of the B-exciton therefore reduces the probability of the double-resonant process, leading to a progressive weakening of the 2LA(M) signal. In contrast, the first-order E and A_1 phonons remain narrow and retain their characteristic symmetry, confirming that the reduction of the 2LA(M) intensity originates from resonance modulation rather than strain-induced structural degradation.

Previous studies generally did not observe a full detuning crossover because the accessible strain ranges were smaller and strain transfer less efficient.^{12,13,21} In our platform, the combination of strong mechanical coupling and strain values exceeding 1% enables us to shift the exciton energy across the entire resonance window. As a result, the detuning-driven collapse of the 2LA(M) band becomes unambiguous (Figure 5(b)).

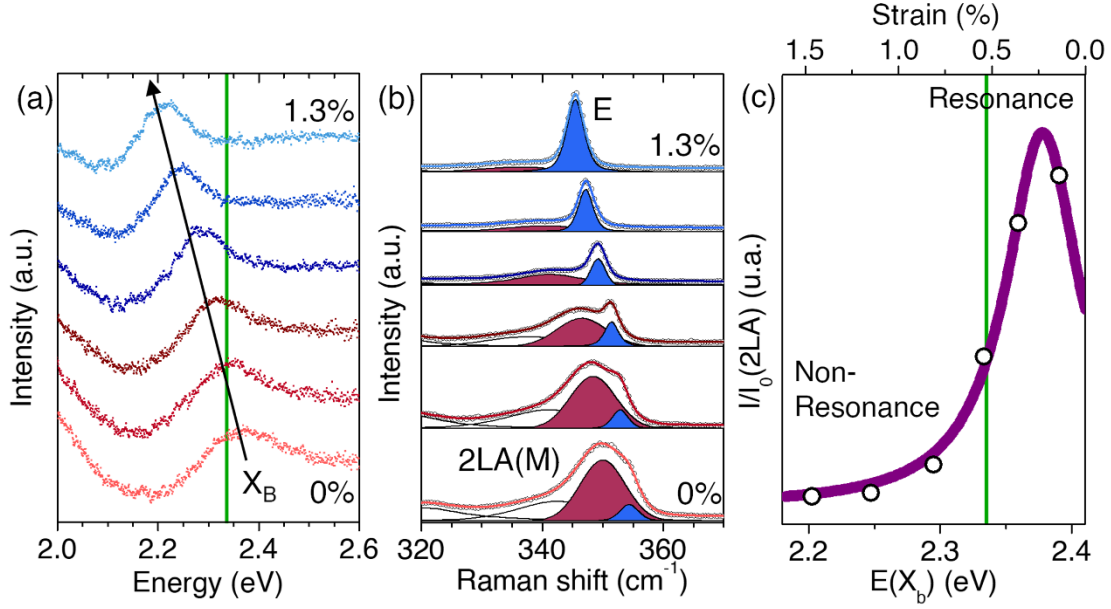


Figure 5. Strain controlled transition between resonant and non-resonant 2LA(M) scattering. (a) B-exciton energy as a function of biaxial strain extracted from differential reflectance. The dashed line indicates the fixed laser energy at 2.33 eV. (b) E and 2LA(M) Raman modes as a function of the biaxial strain. (c) Normalized 2LA(M) intensity as a function of exciton B energy, showing a continuous collapse as the exciton is shifted away from the laser energy (green line). The purple solid line corresponds to the resonance model employed to quantify the detuning-dependent decay of the 2LA(M) intensity.

To describe the strain modulation of the 2LA(M) Raman intensity, we model the resonance directly in terms of the B-exciton energy, $E(X_b)$ which mediates the Raman process. In this framework, the relevant quantity is the energy mismatch between the excitation laser (E_L) and the excitonic intermediate state. Because $E(X_b)$ is obtained experimentally at each strain value, the Raman intensity can be expressed directly as a function of $E(X_b)$ without introducing any explicit dependence on strain. Within semiclassical exciton-mediated Raman theory^{40,41}, the 2LA(M) intensity is described by:

$$I_{2LA(M)} = \frac{A}{(E_L - E(X_b) - \Delta_0)^2 + \Gamma_{\text{eff}}^2}$$

Where A is the exciton-mediated scattering amplitude, Δ_0 is the detuning at which the Raman enhancement is maximal, and Γ_{eff} is the effective resonance width, incorporating both the intrinsic exciton linewidth and additional broadening introduced by the double-resonant process. Fitting the experimental data yields $\Gamma_{\text{eff}} \approx 34$ meV and $\Delta_0 \approx -48$ meV. The negative value of Δ_0 indicates that the 2LA(M) intensity is not maximized at exact exciton-laser alignment. Instead, the resonance peaks when the laser lies approximately 50 meV below the B-exciton energy (Figure 5(c)), which is slightly larger than Γ_{eff} . Consequently, exact laser-exciton alignment already lies on the low-energy shoulder of the resonance, consistent with a phonon-emission-assisted double-resonant process in which the virtual intermediate states lie above the real exciton. The extracted Γ_{eff} defines the energetic window over which 2LA(M) scattering remains resonantly enhanced. Overall, this formulation demonstrates that the modulation of the 2LA(M) intensity is governed by the absolute exciton energy $E(X_b)$, with strain acting solely to shift the exciton through the resonance. This provides direct experimental evidence of strain-controlled exciton-phonon coupling in multilayer WS₂.

The strain-induced transition between resonant and non-resonant scattering in trilayer WS₂ is fully reversible. Upon release of the applied deformation, both the B-exciton energy and the Raman response return to their initial values with no measurable hysteresis (Figure S4). The minimal phonon broadening under strain and the preserved excitonic linewidth confirm that the deformation remains entirely within the elastic regime. The ability to reversibly and continuously tune exciton-phonon interactions, and thereby the Raman scattering cross-section, demonstrates that biaxial strain acts as a reliable and repeatable control parameter. Such mechanically driven modulation of light-matter interactions opens a pathway toward photonic components based on

2D materials. The controlled and quantitative exciton-energy tuning achieved here establishes a general strategy for engineering exciton-mediated optical processes in layered semiconductors. In summary, we demonstrate that biaxial tensile strain provides a robust and reversible means to tune exciton-phonon coupling in trilayer WS₂. By continuously shifting the B-exciton energy relative to the excitation laser, strain drives the system into and out of the double-resonant regime and quantitatively modulates the 2LA(M) intensity. The excellent agreement between experiment and the exciton-energy resonance model establishes a direct link between mechanical deformation, exciton physics and vibrational processes. This approach enables deterministic control of exciton-mediated Raman scattering in two dimensional semiconductors and open a route toward mechanically reconfigurable optical responses, strain-addressable Raman platforms and flexible photonic architectures based on van der Waals materials.

ASSOCIATED CONTENT

Supporting Information.

The Supporting Information includes experimental methods, images of the experimental biaxial setup, additional Raman datasets for monolayer and bilayer WS₂, raw data of differential reflectance spectra, experiments demonstrating the full reversibility of the applied strain under biaxial strain, and details of the theoretical detuning model. (PDF)

AUTHOR INFORMATION

Corresponding Author

Álvaro Rodríguez - Instituto de Ciencia de Materiales de Madrid (ICMM)-Consejo Superior de Investigaciones Científicas (CSIC), C. Sor Juana Inés de la Cruz, 3, 28049 Madrid, Spain; <https://orcid.org/0000-0003-3703-6712>; Email: alvaro.rodriguez@csic.es

Present Addresses

† Álvaro Rodríguez- Departamento de Física de la Materia Condensada, Universidad Autónoma de Madrid, Madrid 28049, Spain and Condensed Matter Physics Center (IFIMAC), Universidad Autónoma De Madrid, Madrid 28049, Spain.

Author Contributions

A.R. conceived the study, fabricated the samples, carried out the experiments, and perform the data analysis. C.M. and A.C.-G. supervised the project and provided guidance on data interpretation and conceptual development. A.R. wrote the manuscript with input and critical feedback from all co-authors. All authors approved the final version of the manuscript.

ACKNOWLEDGMENT

A.R acknowledges funding from the European Union under the Marie Skłodowska-Curie Grant Agreement No.101109987. A.C-G. and C.M. acknowledge support from Grants PDC2023-145920-I00 and PID2023-151946OB-I00, funded by MICIU/AEI/10.13039/501100011033 and, respectively, by the European Union NextGenerationEU/PRTR (PDC2023-145920-I00) and by ERDF/EU (PID2023-151946OB-I00). A.C.-G. also acknowledge funding from the European Research Council (ERC) through the ERC-PoC 2024 StEnSo project (grant agreement 101185235) and the ERC-2024 SyG SKIN2DTRONICS project (grant agreement 101167218).

ICMM-CSIC authors acknowledge support from the Severo Ochoa Centres of Excellence program through Grant CEX2024-001445-S, funded by MICIU/AEI/10.13039/501100011033. ChatGPT was used to improve grammar, clarity overall readability of the manuscript. All outputs were reviewed and revised by the authors prior to inclusion. The authors take full responsibility for the accuracy, interpretation, and overall content of the final manuscript.

REFERENCES

- (1) Niehues, I.; Schmidt, R.; Drüppel, M.; Marauhn, P.; Christiansen, D.; Selig, M.; Berghäuser, G.; Wigger, D.; Schneider, R.; Braasch, L.; Koch, R.; Castellanos-Gomez, A.; Kuhn, T.; Knorr, A.; Malic, E.; Rohlfing, M.; Michaelis de Vasconcellos, S.; Bratschitsch, R. Strain Control of Exciton–Phonon Coupling in Atomically Thin Semiconductors. *Nano Lett.* **2018**, *18* (3), 1751–1757. <https://doi.org/10.1021/acs.nanolett.7b04868>.
- (2) Wang, G.; Chernikov, A.; Glazov, M. M.; Heinz, T. F.; Marie, X.; Amand, T.; Urbaszek, B. Colloquium: Excitons in Atomically Thin Transition Metal Dichalcogenides. *Rev. Mod. Phys.* **2018**, *90* (2), 21001. <https://doi.org/10.1103/RevModPhys.90.021001>.
- (3) Brem, S.; Ekman, A.; Christiansen, D.; Katsch, F.; Selig, M.; Robert, C.; Marie, X.; Urbaszek, B.; Knorr, A.; Malic, E. Phonon-Assisted Photoluminescence from Indirect Excitons in Monolayers of Transition-Metal Dichalcogenides. *Nano Lett.* **2020**, *20* (4), 2849–2856. <https://doi.org/10.1021/acs.nanolett.0c00633>.
- (4) Dadgar, A. M.; Scullion, D.; Kang, K.; Esposito, D.; Yang, E. H.; Herman, I. P.; Pimenta,

- M. A.; Santos, E.-J. G.; Pasupathy, A. N. Strain Engineering and Raman Spectroscopy of Monolayer Transition Metal Dichalcogenides. *Chem. Mater.* **2018**, *30* (15), 5148–5155. <https://doi.org/10.1021/acs.chemmater.8b01672>.
- (5) Peng, Z.; Chen, X.; Fan, Y.; Srolovitz, D. J.; Lei, D. Strain Engineering of 2D Semiconductors and Graphene: From Strain Fields to Band-Structure Tuning and Photonic Applications. *Light Sci. Appl.* **2020**, *9* (1), 190. <https://doi.org/10.1038/s41377-020-00421-5>.
- (6) Hernández López, P.; Heeg, S.; Schattauer, C.; Kovalchuk, S.; Kumar, A.; Bock, D. J.; Kirchof, J. N.; Höfer, B.; Greben, K.; Yagodkin, D.; Linhart, L.; Libisch, F.; Bolotin, K. I. Strain Control of Hybridization between Dark and Localized Excitons in a 2D Semiconductor. *Nat. Commun.* **2022**, *13* (1), 7691. <https://doi.org/10.1038/s41467-022-35352-9>.
- (7) Kumar, A. M.; Yagodkin, D.; Rosati, R.; Bock, D. J.; Schattauer, C.; Tobisch, S.; Hagel, J.; Höfer, B.; Kirchof, J. N.; Hernández López, P.; Burfeindt, K.; Heeg, S.; Gahl, C.; Libisch, F.; Malic, E.; Bolotin, K. I. Strain Fingerprinting of Exciton Valley Character in 2D Semiconductors. *Nat. Commun.* **2024**, *15* (1), 7546. <https://doi.org/10.1038/s41467-024-51195-y>.
- (8) Ronco, G.; Martínez-Suárez, A.; Tedeschi, D.; Savaresi, M.; Hierro-Rodríguez, A.; McVitie, S.; Stroj, S.; Aberl, J.; Brehm, M.; García-Suárez, V. M.; Rota, M. B.; Alonso-González, P.; Martín-Sánchez, J.; Trotta, R. Strain-Induced Exciton Redistribution among Quantum Emitters in Two-Dimensional Materials. *npj 2D Mater. Appl.* **2025**, *9* (1), 65.

<https://doi.org/10.1038/s41699-025-00588-8>.

- (9) Negi, D.; Baishya, M.; Moghe, A. R.; Paul, S.; Badola, S.; Saha, S. Uniaxial Strain-Dependent Resonant Raman Scattering in WS₂. *Small* **2025**, *21* (17), 2412832. <https://doi.org/https://doi.org/10.1002/sml.202412832>.
- (10) Carrascoso, F.; Frisenda, R.; Castellanos-Gomez, A. Biaxial versus Uniaxial Strain Tuning of Single-Layer MoS₂. *Nano Mater. Sci.* **2022**, *4* (1), 44–51. <https://doi.org/https://doi.org/10.1016/j.nanoms.2021.03.001>.
- (11) Kourmoulakis, G.; Michail, A.; Paradisanos, I.; Marie, X.; Glazov, M. M.; Jorissen, B.; Covaci, L.; Stratakis, E.; Papagelis, K.; Parthenios, J.; Kioseoglou, G. Biaxial Strain Tuning of Exciton Energy and Polarization in Monolayer WS₂. *Appl. Phys. Lett.* **2023**, *123* (22), 223103. <https://doi.org/10.1063/5.0167724>.
- (12) Michail, A.; Anestopoulos, D.; Delikoukos, N.; Grammatikopoulos, S.; Tsirkas, S. A.; Lathiotakis, N. N.; Frank, O.; Filintoglou, K.; Parthenios, J.; Papagelis, K. Tuning the Photoluminescence and Raman Response of Single-Layer WS₂ Crystals Using Biaxial Strain. *J. Phys. Chem. C* **2023**, *127* (7), 3506–3515. <https://doi.org/10.1021/acs.jpcc.2c06933>.
- (13) Yang, J. A.; Bennett, R. K. A.; Hoang, L.; Zhang, Z.; Thompson, K. J.; Michail, A.; Parthenios, J.; Papagelis, K.; Mannix, A. J.; Pop, E. Biaxial Tensile Strain Enhances Electron Mobility of Monolayer Transition Metal Dichalcogenides. *ACS Nano* **2024**, *18* (28), 18151–18159. <https://doi.org/10.1021/acsnano.3c08996>.

- (14) Oliva, R.; Wozniak, T.; Faria, P. E. J.; Dybala, F.; Kopaczek, J.; Fabian, J.; Scharoch, P.; Kudrawiec, R. Strong Substrate Strain Effects in Multilayered WS₂ Revealed by High-Pressure Optical Measurements. *ACS Appl. Mater. Interfaces* **2022**, *14* (17), 19857–19868. <https://doi.org/10.1021/acsami.2c01726>.
- (15) Gastaldo, M.; Varillas, J.; Rodríguez, Á.; Velický, M.; Frank, O.; Kalbáč, M. Tunable Strain and Bandgap in Subcritical-Sized MoS₂ Nanobubbles. *npj 2D Mater. Appl.* **2023**, *7* (1), 71. <https://doi.org/10.1038/s41699-023-00432-x>.
- (16) Henríquez-Guerra, E.; Li, H.; Pasqués-Gramage, P.; Gosálbez-Martínez, D.; D'Agosta, R.; Castellanos-Gomez, A.; Calvo, M. R. Large Biaxial Compressive Strain Tuning of Neutral and Charged Excitons in Single-Layer Transition Metal Dichalcogenides. *ACS Appl. Mater. Interfaces* **2023**, *15* (49), 57369–57378. <https://doi.org/10.1021/acsami.3c13281>.
- (17) Manzanares-Negro, Y.; Zambudio, A.; López-Polín, G.; Sarkar, S.; Chhowalla, M.; Gómez-Herrero, J.; Gómez-Navarro, C. Fatigue Response of MoS₂ with Controlled Introduction of Atomic Vacancies. *Nano Lett.* **2023**, *23* (23), 10731–10738. <https://doi.org/10.1021/acs.nanolett.3c02479>.
- (18) Stellino, E.; D'Alò, B.; Blundo, E.; Postorino, P.; Polimeni, A. Fine-Tuning of the Excitonic Response in Monolayer WS₂ Domes via Coupled Pressure and Strain Variation. *Nano Lett.* **2024**, *24* (13), 3945–3951. <https://doi.org/10.1021/acs.nanolett.4c00157>.
- (19) Harats, M. G.; Kirchhof, J. N.; Qiao, M.; Greben, K.; Bolotin, K. I. Dynamics and

- Efficient Conversion of Excitons to Trions in Non-Uniformly Strained Monolayer WS₂. *Nat. Photonics* **2020**, *14* (5), 324–329. <https://doi.org/10.1038/s41566-019-0581-5>.
- (20) Rodriguez, A.; Kalbáč, M.; Frank, O. Strong Localization Effects in the Photoluminescence of Transition Metal Dichalcogenide Heterobilayers. *2D Mater.* **2021**, *8* (2), 025028. <https://doi.org/10.1088/2053-1583/abe363>.
- (21) Roy, S.; Yang, X.; Gao, J. Biaxial Strain Tuned Upconversion Photoluminescence of Monolayer WS₂. *Sci. Rep.* **2024**, *14* (1), 3860. <https://doi.org/10.1038/s41598-024-54185-8>.
- (22) Waheed, Y.; Shit, S.; Surendran, J. T.; Prasad, I. D.; Watanabe, K.; Taniguchi, T.; Kumar, S. Large Trion Binding Energy in Monolayer WS₂ via Strain-Enhanced Electron–Phonon Coupling. *Commun. Mater.* **2025**, *6* (1), 86. <https://doi.org/10.1038/s43246-025-00809-z>.
- (23) Liu, H.-L.; Yang, T.; Tatsumi, Y.; Zhang, Y.; Dong, B.; Guo, H.; Zhang, Z.; Kumamoto, Y.; Li, M.-Y.; Li, L.-J.; Saito, R.; Kawata, S. Deep-Ultraviolet Raman Scattering Spectroscopy of Monolayer WS₂. *Sci. Rep.* **2018**, *8* (1), 11398. <https://doi.org/10.1038/s41598-018-29587-0>.
- (24) del Corro, E.; Botello-Méndez, A.; Gillet, Y.; Elias, A. L.; Terrones, H.; Feng, S.; Fantini, C.; Rhodes, D.; Pradhan, N.; Balicas, L.; Gonze, X.; Charlier, J.-C.; Terrones, M.; Pimenta, M. A. Atypical Exciton–Phonon Interactions in WS₂ and WSe₂ Monolayers Revealed by Resonance Raman Spectroscopy. *Nano Lett.* **2016**, *16* (4), 2363–2368. <https://doi.org/10.1021/acs.nanolett.5b05096>.

- (25) Molas, M. R.; Nogajewski, K.; Potemski, M.; Babiński, A. Raman Scattering Excitation Spectroscopy of Monolayer WS₂. *Sci. Rep.* **2017**, *7* (1), 5036. <https://doi.org/10.1038/s41598-017-05367-0>.
- (26) Zhao, W.; Ghorannevis, Z.; Amara, K. K.; Pang, J. R.; Toh, M.; Zhang, X.; Kloc, C.; Tan, P. H.; Eda, G. Lattice Dynamics in Mono- and Few-Layer Sheets of WS₂ and WSe₂. *Nanoscale* **2013**, *5* (20), 9677–9683. <https://doi.org/10.1039/C3NR03052K>.
- (27) Magda, G. Z.; Petó, J.; Dobrik, G.; Hwang, C.; Biró, L. P.; Tapasztó, L. Exfoliation of Large-Area Transition Metal Chalcogenide Single Layers. *Sci. Rep.* **2015**, *5* (1), 14714. <https://doi.org/10.1038/srep14714>.
- (28) Velický, M.; Donnelly, G. E.; Hendren, W. R.; McFarland, S.; Scullion, D.; DeBenedetti, W. J. I.; Correa, G. C.; Han, Y.; Wain, A. J.; Hines, M. A.; Muller, D. A.; Novoselov, K. S.; Abruña, H. D.; Bowman, R. M.; Santos, E. J. G.; Huang, F. Mechanism of Gold-Assisted Exfoliation of Centimeter-Sized Transition-Metal Dichalcogenide Monolayers. *ACS Nano* **2018**, *12* (10), 10463–10472. <https://doi.org/10.1021/acsnano.8b06101>.
- (29) Velický, M.; Rodriguez, A.; Bouša, M.; Krayev, A. V.; Vondráček, M.; Honolka, J.; Ahmadi, M.; Donnelly, G. E.; Huang, F.; Abruña, H. D.; Novoselov, K. S.; Frank, O. Strain and Charge Doping Fingerprints of the Strong Interaction between Monolayer MoS₂ and Gold. *J. Phys. Chem. Lett.* **2020**, *11* (15), 6112–6118. <https://doi.org/10.1021/acs.jpcllett.0c01287>.
- (30) Rodríguez, Á.; Çakiroğlu, O.; Li, H.; Carrascoso, F.; Mompean, F.; Garcia-Hernandez,

- M.; Munuera, C.; Castellanos-Gomez, A. Improved Strain Transfer Efficiency in Large-Area Two-Dimensional MoS₂ Obtained by Gold-Assisted Exfoliation. *J. Phys. Chem. Lett.* **2024**, *15* (24), 6355–6362. <https://doi.org/10.1021/acs.jpcclett.4c00855>.
- (31) Androulidakis, C.; Koukaras, E. N.; Parthenios, J.; Kalosakas, G.; Papagelis, K.; Galiotis, C. Graphene Flakes under Controlled Biaxial Deformation. *Sci. Rep.* **2015**, *5* (1), 18219. <https://doi.org/10.1038/srep18219>.
- (32) Michail, A.; Anestopoulos, D.; Delikoukos, N.; Parthenios, J.; Grammatikopoulos, S.; Tsirkas, S. A.; Lathiotakis, N. N.; Frank, O.; Filintoglou, K.; Papagelis, K. Biaxial Strain Engineering of CVD and Exfoliated Single- and Bi-Layer MoS₂ Crystals. *2D Mater.* **2021**, *8* (1), 15023. <https://doi.org/10.1088/2053-1583/abc2de>.
- (33) Rodriguez, A.; Velický, M.; Řáhová, J.; Zólyomi, V.; Koltai, J.; Kalbáč, M.; Frank, O. Activation of Raman Modes in Monolayer Transition Metal Dichalcogenides through Strong Interaction with Gold. *Phys. Rev. B* **2022**, *105* (19), 195413. <https://doi.org/10.1103/PhysRevB.105.195413>.
- (34) Chen, S.-Y.; Zheng, C.; Fuhrer, M. S.; Yan, J. Helicity-Resolved Raman Scattering of MoS₂, MoSe₂, WS₂, and WSe₂ Atomic Layers. *Nano Lett.* **2015**, *15* (4), 2526–2532. <https://doi.org/10.1021/acs.nanolett.5b00092>.
- (35) Berkdemir, A.; Gutiérrez, H. R.; Botello-Méndez, A. R.; Perea-López, N.; Elías, A. L.; Chia, C.-I.; Wang, B.; Crespi, V. H.; López-Urías, F.; Charlier, J.-C.; Terrones, H.; Terrones, M. Identification of Individual and Few Layers of WS₂ Using Raman

- Spectroscopy. *Sci. Rep.* **2013**, 3 (1), 1755. <https://doi.org/10.1038/srep01755>.
- (36) Mohiuddin, T. M. G.; Lombardo, A.; Nair, R. R.; Bonetti, A.; Savini, G.; Jalil, R.; Bonini, N.; Basko, D. M.; Galiotis, C.; Marzari, N.; Novoselov, K. S.; Geim, A. K.; Ferrari, A. C. Uniaxial Strain in Graphene by Raman Spectroscopy: G Peak Splitting, Grüneisen Parameters, and Sample Orientation. *Phys. Rev. B* **2009**, 79 (20), 205433. <https://doi.org/10.1103/PhysRevB.79.205433>.
- (37) del Corro, E.; de la Roza, A. O.; Taravillo, M.; Baonza, V. G. Raman Modes and Grüneisen Parameters of Graphite under Compressive Biaxial Stress. *Carbon N. Y.* **2012**, 50 (12), 4600–4606. <https://doi.org/https://doi.org/10.1016/j.carbon.2012.05.046>.
- (38) Frisenda, R.; Drüppel, M.; Schmidt, R.; Michaelis de Vasconcellos, S.; Perez de Lara, D.; Bratschitsch, R.; Rohlfing, M.; Castellanos-Gomez, A. Biaxial Strain Tuning of the Optical Properties of Single-Layer Transition Metal Dichalcogenides. *npj 2D Mater. Appl.* **2017**, 1 (1), 10. <https://doi.org/10.1038/s41699-017-0013-7>.
- (39) Zollner, K.; Junior, P. E. F.; Fabian, J. Strain-Tunable Orbital, Spin-Orbit, and Optical Properties of Monolayer Transition-Metal Dichalcogenides. *Phys. Rev. B* **2019**, 100 (19), 195126. <https://doi.org/10.1103/PhysRevB.100.195126>.
- (40) Shi, L.; Rohringer, P.; Wanko, M.; Rubio, A.; Waßerroth, S.; Reich, S.; Cambré, S.; Wenseleers, W.; Ayala, P.; Pichler, T. Electronic Band Gaps of Confined Linear Carbon Chains Ranging from Polyyne to Carbyne. *Phys. Rev. Mater.* **2017**, 1 (7), 75601. <https://doi.org/10.1103/PhysRevMaterials.1.075601>.

- (41) Heeg, S.; Shi, L.; Pichler, T.; Novotny, L. Raman Resonance Profile of an Individual Confined Long Linear Carbon Chain. *Carbon N. Y.* **2018**, *139*, 581–585.
<https://doi.org/https://doi.org/10.1016/j.carbon.2018.07.007>.